THEMATIC ISSUE

The deep thermal field of the Glueckstadt Graben

**Philipp Balling · Yuriy Maystrenko ·
Magdalena Scheck-Wenderoth**

Abstract With this paper, we assess the present-day conductive thermal field of the Glueckstadt Graben in NW Germany that is characterized by large salt walls and diapirs structuring the graben fill. We use a finite element method to calculate the 3D steady-state conductive thermal field based on a lithosphere-scale 3D structural model that resolves the first-order structural characteristics of the graben and its underlying lithosphere. Model predictions are validated against measured temperatures in six deep wells. Our investigations show that the interaction of thickness distributions and thermal rock properties of the different geological layers is of major importance for the distribution of temperatures in the deep subsurface of the Glueckstadt Graben. However, the local temperatures may result from the superposed effects of different controlling factors. Especially, the upper sedimentary part of the model exhibits huge lateral temperature variations, which correlate spatially with the shape of the thermally highly conductive Permian salt layer. Variations in thickness and geometry of the salt cause two major effects, which provoke considerable lateral temperature variations for a given depth. (1) The "chimney effect" causes more efficient heat transport within salt diapirs. As a consequence positive thermal anomalies develop in the upper part and above salt structures, where the latter are covered by much less conductive sediments. In contrast, negative thermal anomalies are noticeable underneath salt structures. (2) The "thermal blanketing effect" is caused by thermally low conductive sediments that provoke the local storage of heat where these insulating sediments are present. The latter effect leads to both local and regional thermal anomalies. Locally, this translates to higher temperatures where salt margin synclines are filled with thick insulating clastic sediments. For the regional anomalies the cumulative insulating effects of the entire sediment fill results in a long-wavelength variation of temperatures in response to heat refraction effects caused by the contrast between insulating sediments and highly conductive crystalline crust. Finally, the longest wavelength of temperature variations is caused by the depth position of the isothermal lithosphere–asthenosphere boundary defining the regional variations of the overall geothermal gradient. We find that a conductive thermal model predicts observed temperatures reasonably well for five of the six available wells, whereas the steady-state conductive approach appears not to be valid for the sixth well.

P. Balling (✉)
Institute of Earth and Environmental Science, University of Potsdam, 14476 Potsdam-Golm, Germany
e-mail: balling@uni-potsdam.de

Y. Maystrenko · M. Scheck-Wenderoth
Helmholtz Centre Potsdam, GFZ German Research Centre for Geosciences, Telegrafenberg, 14473 Potsdam, Germany
e-mail: yuriy.maystrenko@ngu.no

M. Scheck-Wenderoth
e-mail: leni@gfz-potsdam.de

Y. Maystrenko
Geological Survey of Norway (NGU), Trondheim, Norway

Introduction

In times of global sustainable energy production and advanced methods for the investigation of the subsurface, geothermal energy is of growing interest. Therewith 3D modelling is a tool, which will get more important for fast and cheap analysis of datasets of the Earth's interior. Especially in the field of temperature distribution of the subsurface numerical models provide a predictive alternative to conventional expensive drilling methods. We present results from 3D thermal finite element models of Schleswig–Holstein in North-West Germany. The study area (Figs. 1, 2) encompasses the whole Glueckstadt Graben, which is one of the deepest post-Permian sub-basins of the Central European Basin System (CEBS). Accordingly, the Glueckstadt Graben has a comparable geological history and stratigraphy like the surrounding basins, as the adjacent North-East German Basin, the Horn Graben (HG) and the Lower Saxony Basin (Fig. 1). The Glueckstadt Graben is proper bounded to the north by the Ringkoebing-Fyn High (Fig. 1), to the south by the Pompeckj block (Fig. 2), to the west by the North Sea and to the east by the Baltic Sea. This area is located between the Caledonian Deformation Front to the north and the Elbe Fault System to the south (Fig. 1). The Glueckstadt Graben contains a more than 10 km thick Permian to Cenozoic infill that rests on a Devonian–Carboniferous and possibly older sedimentary sequence and a Caledonian consolidated crystalline crust (Bayer et al. 2002). Internally, the morphology and infill of the Glueckstadt Graben was strongly controlled by movements of the Permian salt, which formed salt pillows, domes and walls, with a relief of more than 9,000 m (Figs. 2, 3). The formation of these salt structures also affected the style of deposition in the past. Thereby, thickest sediments were deposited around salt structures and this sediment down-building, in turn, enhanced the growth of salt structures. The Central Glueckstadt Graben is the deepest (up to 10 km depth) post-Permian structural feature, flanked by rim synclines, in the south-east by the Hamburg trough, in the north-east by the Eastholstein trough and in the north-west by the Westholstein trough (Fig. 2) (Maystrenko et al. 2005a).

Since the beginning of the last century, the present-day tectonic setting and the infill of the Glueckstadt Graben were intensively studied by oil and gas exploration companies but also by numerous academic research projects (Trusheim 1960; Sannemann 1968; Jaritz 1969, 1980; Best et al. 1983; Brink et al. 1990, 1992; Baldschuhn et al. 1996, 2001; Maystrenko et al. 2005a, b, 2006; Yoon et al. 2008). According to the studies of Brink et al. (1990), Ziegler (1992) and Maystrenko et al. (2006), the Glueckstadt Graben developed out of an underlying Permian Basin, which formed during Late Carboniferous–Early Permian
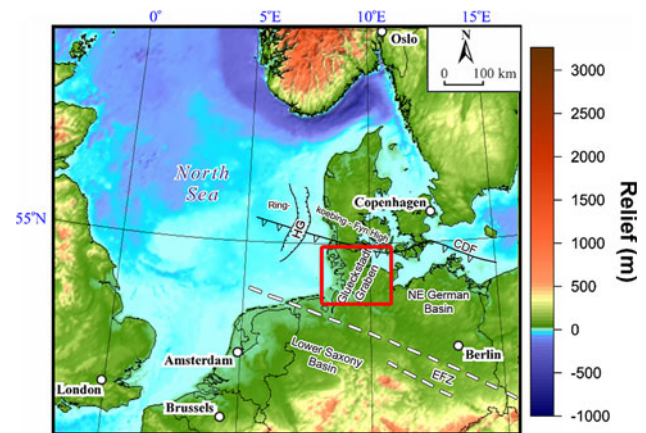

Fig. 1 Location of the Glueckstadt Graben (*red frame*), North-East German Basin, the Horn Graben (HG), Lower Saxony Basin, Ringkoebing-Fyn High, Caledonian deformation front (CDF) Elbe fault system (EFZ)
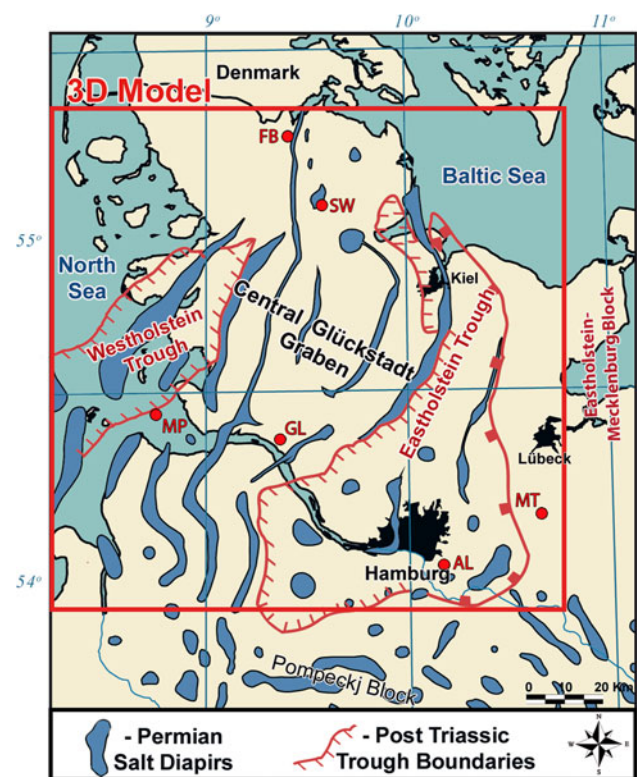
Fig. 2 Simplified tectonic map of the Glueckstadt Graben, showing salt diapirs, the location of the Pompeckj block (Baldschuhn et al. 1996) and well locations in the study area (Modified after Maystrenko et al. 2005a). *AL* Allermöhe, *FB* Flensburg Z1, *GL* Glückstadt T1, *MP* Mittelplate 2, *MT* Moelln Tief 1, *SW* Schleswig Z1

times. The evolution of the Glueckstadt Graben can be described in four major phases: (1) pre-Permian deposition, (2) late Carboniferous–Early Permian rifting, (3) post-rift thermal subsidence lasting from the Late Permian into Early Triassic times and (4) the Meso–Cenozoic development (Maystrenko et al. 2006). While the pre-Permian

Fig. 3 Relief of the top
Permian salt (Zechstein and
Rotliegend salt) after
Baldschuhn et al. (1996, 2001).
Model coordinates are based on
the Gauss-Krueger DHDN
(zone 3) system using the WGS
84 datum
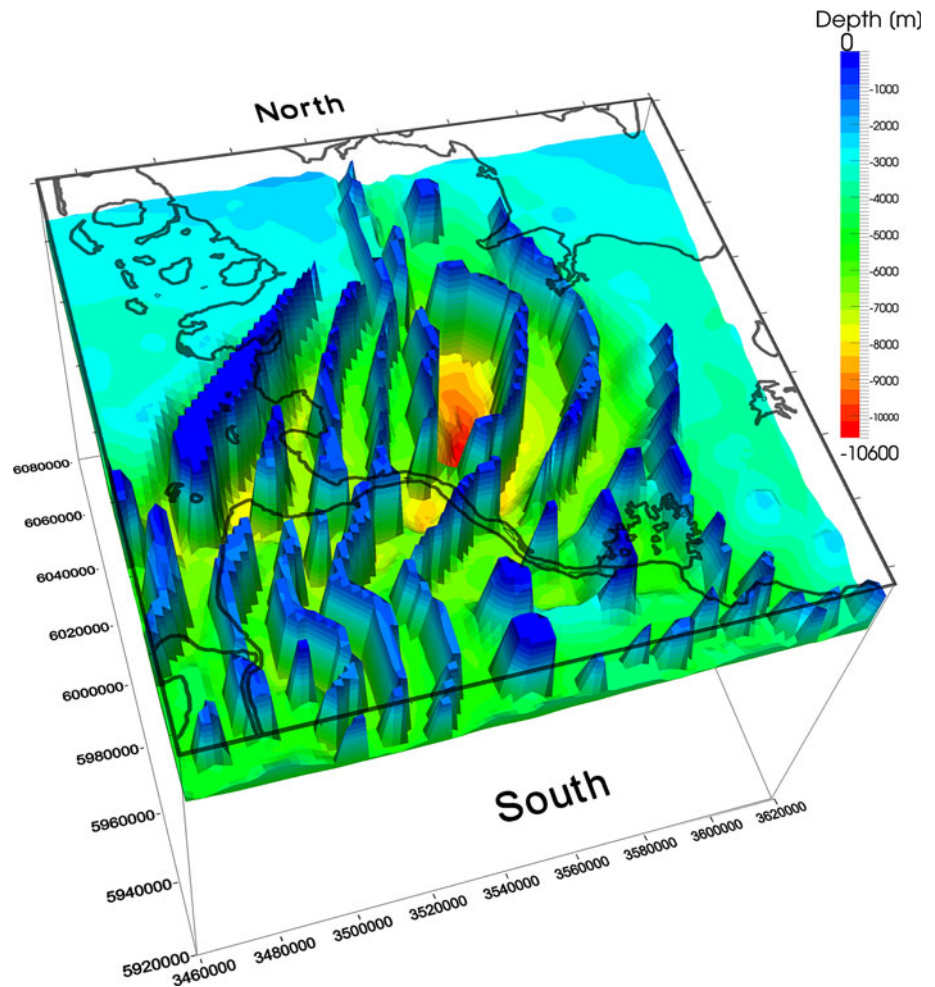
depositional phase was largely detached from the later structural evolution of the basin, the phase of thermal subsidence gave way to the deposition of the Permian evaporites that have been mobilized in the Mesozoic and Cenozoic times. Permian salt consists of a lower sequence of Upper Rotliegend salt and more important, initially up to 2.5 km thick (Maystrenko et al. 2005b, 2013) sequence of Zechstein salt. These layers are composed dominantly of rock salt, which on geological time scales behaves viscously. This property together with the low density of rock salt led to a destabilization of the salt layer in response to changing stress fields or changing overburden load. Salt rise may have passed through several stages and culminated in the piercing of the post-salt cover in many places. Accordingly, the present-day structural configuration of the Glueckstadt Graben has been shaped during the Triassic to Cenozoic interplay of salt movement and depositional response.

Earlier studies (Maystrenko et al. 2005a, b, 2006) integrated a large amount of geological and geophysical data into a consistent 3D structural model of the Glueckstadt Graben. Moreover, regional 3D structural models on the

scale of the lithosphere have been derived (Maystrenko and Scheck-Wenderoth 2013). With this study, we combine the available structural models into a 3D, lithosphere-scale structural model of the Glueckstadt Graben that we use as a basis for 3D calculations of the conductive thermal field. We validate different calculated model approaches with measured temperatures observed in six deep wells and test the sensitivity of the models with respect to the assigned physical properties. Finally, we discuss the implications of the best-fit model with respect to controlling factors for subsurface temperature distribution.

The 3D structural model

For the calculation of the 3D conductive thermal field of the Glueckstadt Graben, two different structural models were combined into one. For the upper (sedimentary rock) part, the structural model of the Glueckstadt Graben was taken from an earlier model (Maystrenko et al. 2006), which integrates two-dimensional structural depth maps from the Geotectonic Atlas of NW Germany (Baldschuhn

et al. [1996], [2001]). For the lower part from the base of the lower Permian Rotliegend to the LAB (Lithosphere–Asthenosphere Boundary), another model was taken from Maystrenko and Scheck-Wenderoth ([2013]). Both models were combined into one lithosphere-scale 3D structural model of the Glueckstadt Graben. The final combined model extends from 53.4°N to 54.8°N latitude and 8.2°E to 10.8°E longitude and covers an area of 170 km and 166 km. Thereby, it contains 15 layers (Figs. [4], [5], [6], [7]; Table [1]): Quaternary/Neogene, Paleogene, Upper Cretaceous, Lower Cretaceous, Jurassic, Keuper, Muschelkalk, Buntsandstein, Permian salt (Zechstein and salt-rich Rotliegend), Rotliegend, Permo-Carboniferous volcanics, pre-Permian sediments, upper crystalline crust, lower crystalline crust and lithospheric mantle. The model extends vertically down to a depth of about 120 km. Thereby, its vertical resolution corresponds to the number of the differentiated geological units. The horizontal resolution is 2 km, allowing a good representation of geological structures, in particular resolving the major salt structures. Model coordinates are based on the Gauss-Krueger DHDN (zone 3) system using the WGS 84 datum.

Configuration of the post-salt units

Due to continued thermal subsidence of the basin, the Zechstein salt had been completely buried by more than 1,000 m thick clastic Buntsandstein sediments in the Early Triassic. Sand and clay are the main clastic components of the Buntsandstein. Coevally, extensional stresses (Brink et al. [1990]; Kockel [2002]; Maystrenko et al. [2005b]) initiated earliest salt movements. Higher temperature, pressure and (re)activation of faults intensified the viscous behaviour of the Permian salt and halokinesis began (Trusheim [1960]; Sannemann [1965], [1968]). Salt pillows formed along strike of normal faults (Maystrenko et al. [2005b]). As a consequence, rim synclines were formed at the edge of salt pillows, which caused a reactivation of faults and started the formation of salt diapirs and walls (Sannemann [1965]). The vast majority of Buntsandstein sediments are located in the Central Glueckstadt Graben (Fig. [6]h) where they attain a thickness of up to 2,000 m. The top of this layer is deepest in the Westholstein trough and in the Central Glueckstadt Graben (Fig. [4]h) at present day. The thickness of the overlying Muschelkalk carbonates also indicates subsidence and salt withdrawal from the Central Glueckstadt Graben (Fig. [6]g) and again, the top of this layer is deepest in the Westholstein trough and in the Central Glueckstadt Graben (Fig. [4]g) today.

The main Mesozoic extensional phase occurred in Late Triassic times (Keuper), leading to intensive normal faulting and salt rise within the N–S striking Central Glueckstadt Graben where the former cover was pierced by the rising salt. During this time, the salt layer was depleted in the central part of the Graben. In the resulting accommodation space, thick Keuper sediments were deposited with a regional present-day thickness of more than 5,000 m (Fig. [6]f). This deposition of clay, marl and gypsum reinforced the growth of salt structures. The present-day top of the Keuper layer is deepest in the Westholstein, Eastholstein and Hamburg troughs (Fig. [4]f). No Keuper sediments are found on top of salt walls (blue structures in the Central Glueckstadt Graben) and the salt even may have extruded at the surface during this time interval (Trusheim [1960]; Maystrenko et al. [2005a]). The constant thickness of the Keuper at the flanks of the Glueckstadt Graben suggests that the Eastholstein and Mecklenburg Blocks (Fig. [2]) were not significantly deformed by the Late Triassic extensional event (Baldschuhn et al. [2001]; Maystrenko et al. [2005b]).

Salt rise also controlled the deposition of the Jurassic sediments around forming salt diapirs (Maystrenko et al. [2005b]). The Jurassic sediments are made of clay, sand, silt and marl and the preserved thickness of this unit shows maxima marginal to the Central Glueckstadt Graben parallel to the most marginal salt structures of the latter. As a result the deepest and thickest Jurassic rocks can be found in the Westholstein and Hamburg troughs (Figs. [4]e, [6]e). In addition, during Jurassic the Glueckstadt Graben was affected by an erosional event, expressed as a Late Jurassic–earliest Early Cretaceous regional unconformity. Today Lower Cretaceous deposits, mainly consisting of clay, sand and silt, are found with an average regional thickness of about 60–120 m (in the Westholstein and Hamburg troughs up to 520 m) within the limits of the Glueckstadt Graben (Fig. [6]d). The thickest parts of preserved Lower Cretaceous are evident in the Westholstein trough and in the south around a salt diapir whereas the top of this layer is deepest in the Westholstein and Hamburg troughs (Fig. [4]d).

The upper Cretaceous unit consists of chalky limestones characterized by a uniform lithology. The layer has an almost constant thickness of about 900 m over the entire study area covering most of the previous salt structures, apart from a moderate thickening in the Westholstein and Eastholstein troughs (Fig. [6]c). Deposition occurred in a gentle platform-type depression and extended far beyond the boundaries of the Glueckstadt Graben. The top of this layer is deepest in the Westholstein and Hamburg troughs (Fig. [4]c). Indications for Late Cretaceous–Early Cenozoic inversion observed over large parts of North Central Europe are weak to absent for the area of the Glueckstadt Graben (Maystrenko et al. [2005b]; Scheck-Wenderoth and Maystrenko [2008]). In contrast, indications for regional W-E-directed Paleogene–Neogene extension in terms of active normal faulting and renewed salt mobilization point
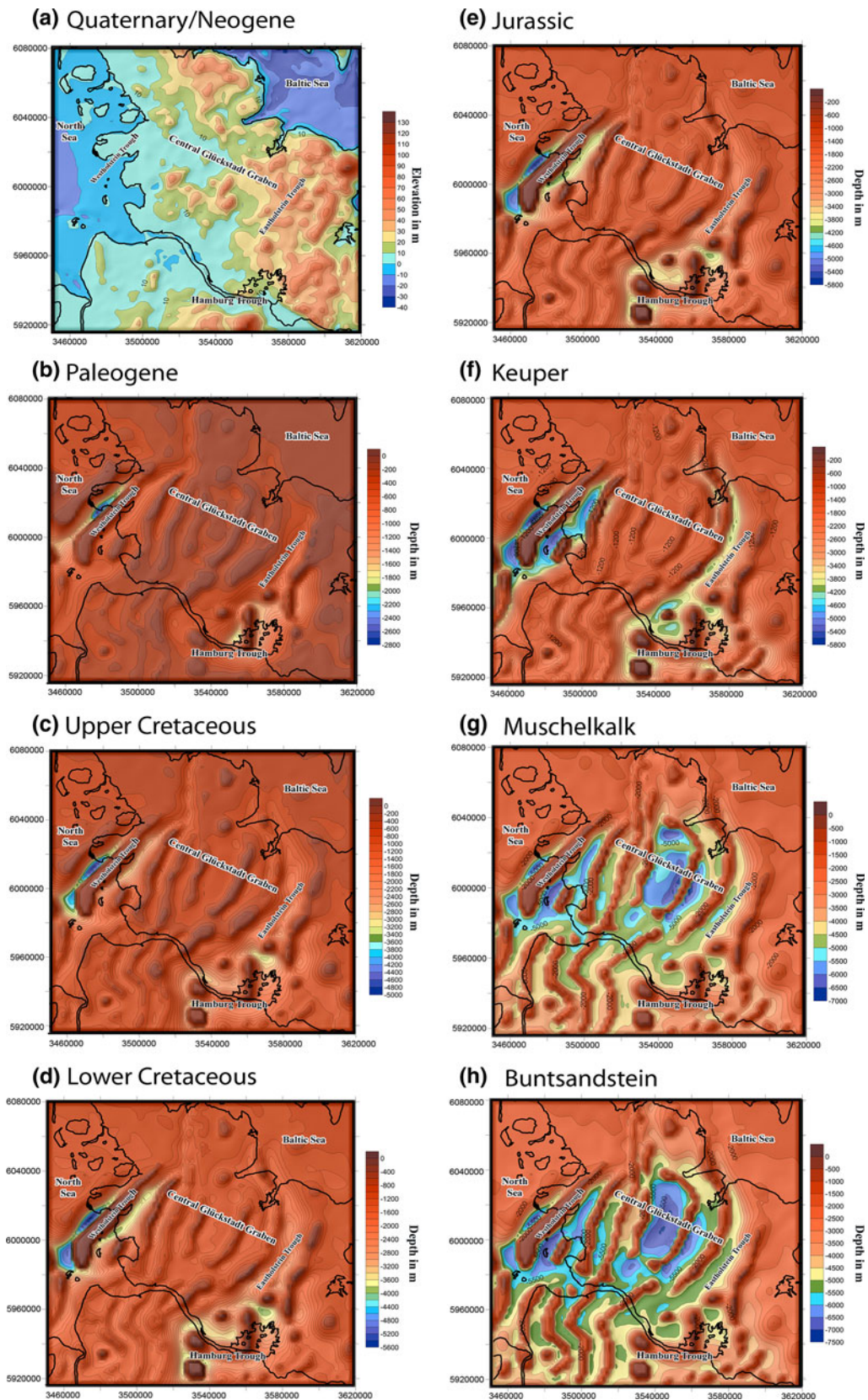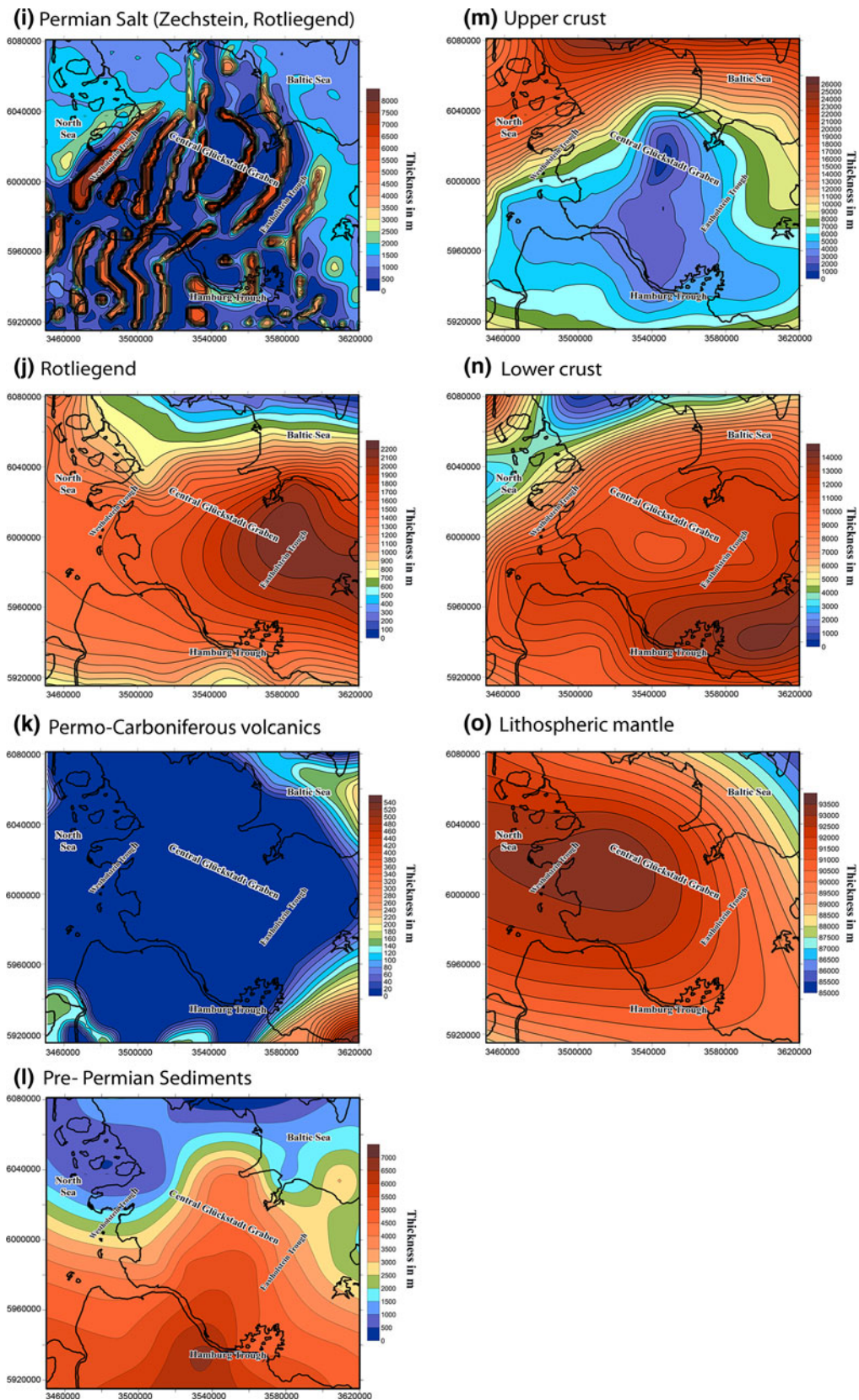
Fig. 4 Depth of the top of the post-Permian salt stratigraphic layer in the 3D model. Model coordinates are based on the Gauss-Krueger DHDN (zone 3) system using the WGS 84 datum
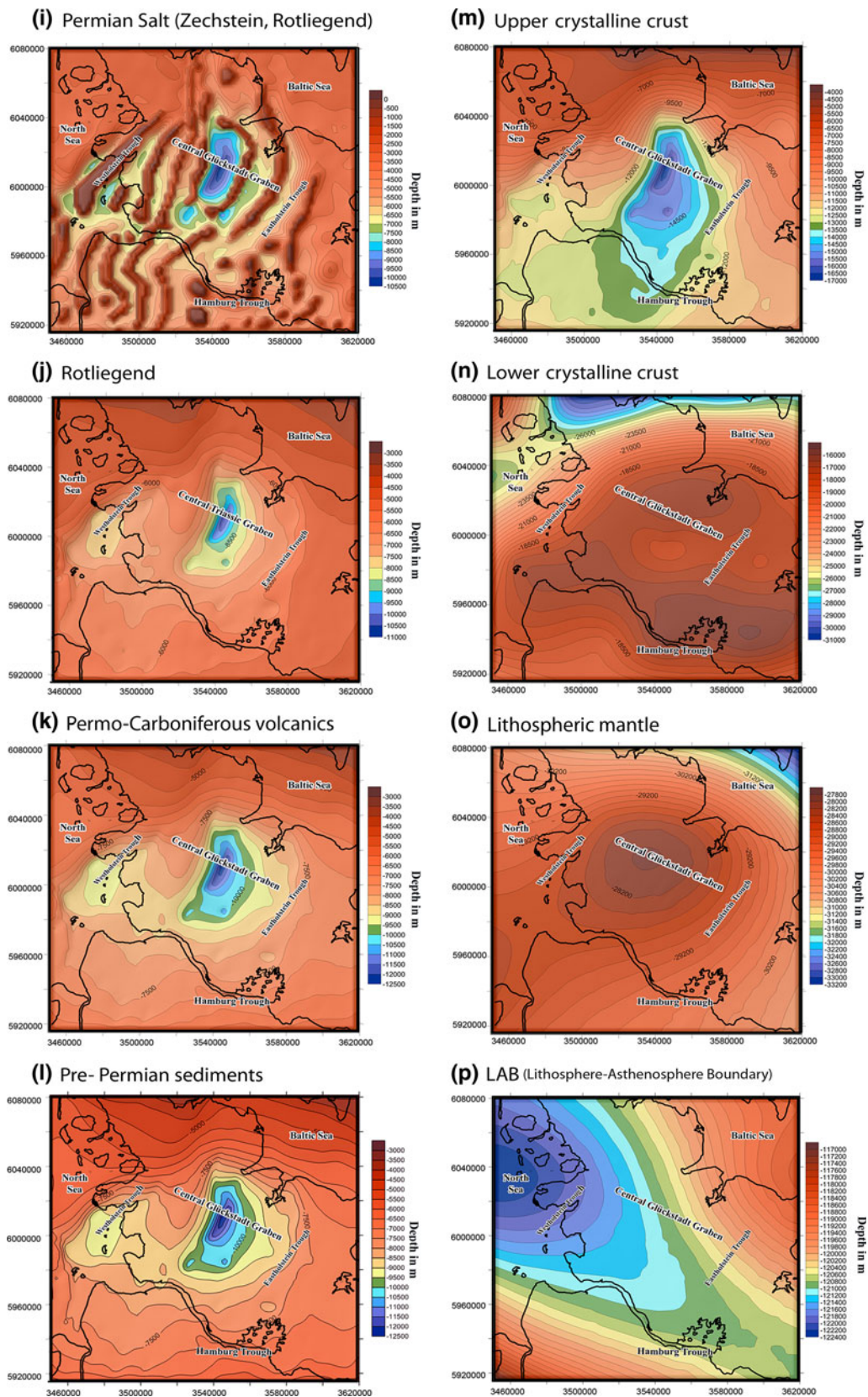
Fig. 5 Depth of the top of the Permian salt and pre-Permian salt stratigraphic layer in the 3D model. Model coordinates are based on the Gauss-Krueger DHDN (zone 3) system using the WGS 84 datum
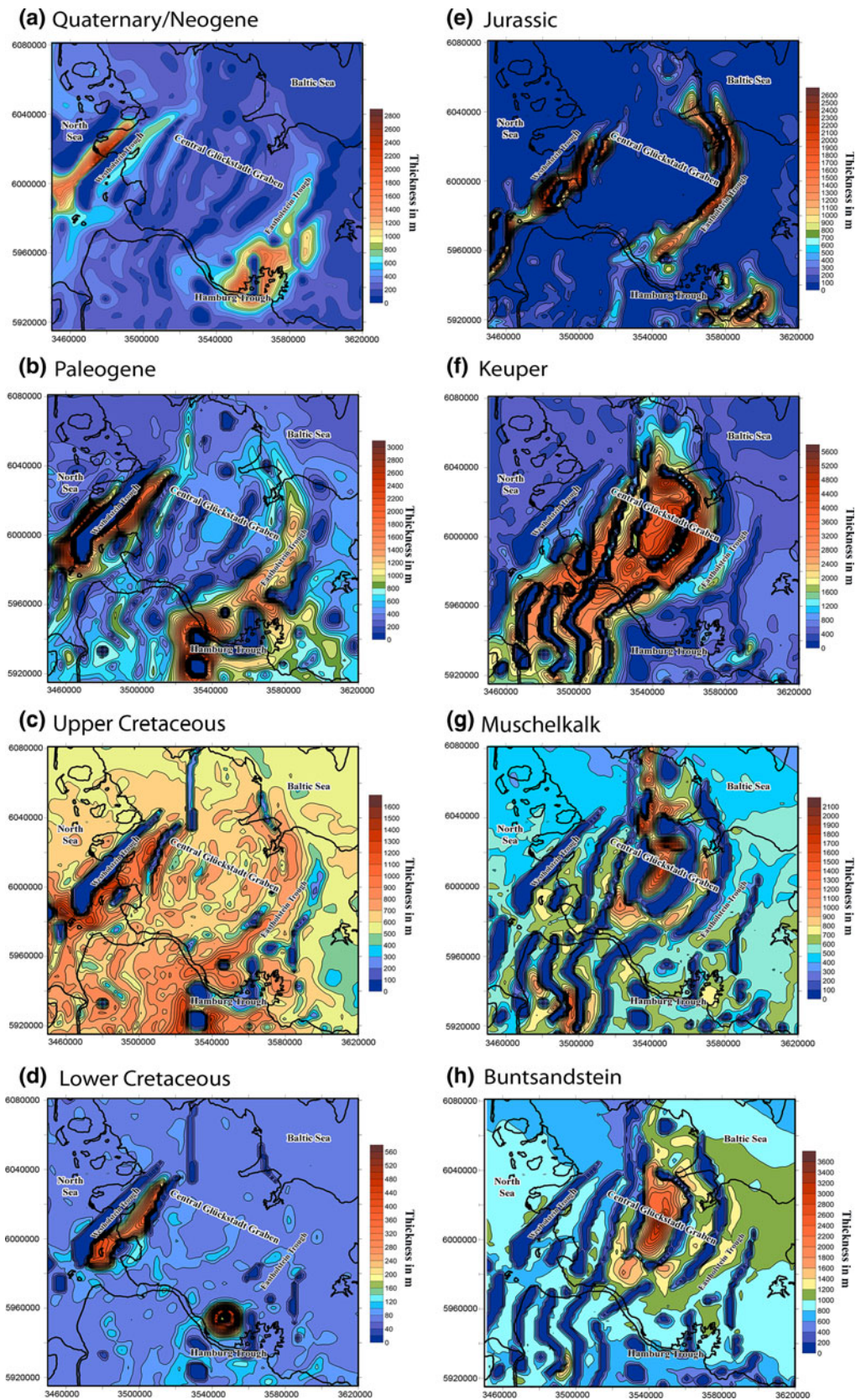
Fig. 6 Isopachs of the post-Permian salt stratigraphic layer in the 3D model. Model coordinates are based on the Gauss-Krueger DHDN (zone 3) system using the WGS 84 datum

Fig. 7 Isopachs of the Permian salt and pre-Permian salt stratigraphic layer in the 3D model. Model coordinates are based on the Gauss-Krueger DHDN (zone 3) system using the WGS 84 datum

Table 1 Stratigraphic units, their corresponding dominant lithology, the input parameters of the first calculation taken from (Noack et al. 2012) and for the final (best-fit) calculation

Stratigraphic unit	Dominant lithology	1st calculation reference model (Noack et al. 2012)		Final calculation best-fit model	
		λ (W/m K)	S (W/m^3)	λ (W/m K)	S (W/m^3)
Cenozoic (Neogene, Paleogene)	Sand, silt and clay	1.5	0.7e−06	**1.5**	**0.7e−06**
Upper Cretaceous	Limestone	1.9	0.3e−06	**2.1**	**0.3e−06**
Lower Cretaceous	Clay interbedded with sand, silt	2.0	1.4e−06	**1.5**	**1.4e−06**
Jurassic	Clay interbedded with sand, silt and marl	2.0	1.4e−06	**1.8**	**1.4e−06**
Keuper	Clay with marl, gypsum	2.3	1.4e−06	**2.4**	**1.4e−06**
Muschelkalk	Carbonates	1.85	0.3e−06	**1.9**	**0.4e−06**
Buntsandstein	Silts with sand and clay	2.0	1.0e−06	**1.6**	**1.5e−06**
Permian salt	Evaporites (mainly salt)	3.5	0.09e−06	**3.5**	**0.09e−06**
Rotliegend	Clay, silt and clay	2.16	1.0e−06	**2.16**	**1.0e−06**
Permo-Carboniferous volcanics	Rhyolithe and andesite	2.5	2.0e−06	**2.5**	**2.0e−06**
Pre-Permian sediments	Clastics (strongly compacted)	2.65	1.5e−06	**2.65**	**1.5e−06**
Upper crystalline crust	Granitoids	3.1	2.5e−06	**2.8**	**1.2e−06**
Lower crystalline crust	Gabbro	2.7	0.8e−06	**2.9**	**0.7e−06**
Lithospheric mantle	Peridotite	3.95	0.03e−06	**3.95**	**0.03e−06**

to a change in the tectonic regime after the Late Cretaceous–Early Cenozoic compression (Maystrenko et al. 2005a, 2006). Accordingly, regional thickness variations of the Paleogene point to renewed salt movements and thickest sediments are found in the Westholstein and Hamburg troughs (Fig. 6b). The Paleogene sediments consist of sand, silt and clay and the top of this layer are deepest in the Westholstein and Hamburg troughs (Fig. 4b). The uppermost layer of the model is the Quaternary–Neogene composed mainly of sand, silt and clay. This youngest layer is characterized by largest thicknesses in the Westholstein and Hamburg troughs (Fig. 6a). Its top coincides with present-day topography/bathymetry (Fig. 4a), which shows only moderate variations of ±100 m.

Configuration of the salt and pre-salt units

The isopach map of the Permian salt (Fig. 7i) shows a structural trend in terms of SSW-NNE striking salt structures. A combined inspection of the top salt depth contours (Fig. 5i) and of the salt isopach map reveals that the salt walls can be a few km wide, up to 9 km high and may extend in N–S direction over more than 100 km.

Below the salt, the structural pattern changes completely. The sedimentary Lower Permian Rotliegend rocks are composed of clay and silt. Neither the thickness distribution (Fig. 7j) of this layer nor the relief of its top (Fig. 5j) displays the short-wavelength variations of the salt and post-salt layers as the sub-salt layers were not

affected by salt movements. The thickness map (Fig. 7j) shows that the thickest Rotliegend is modelled in the Eastholstein trough whereas the top Rotliegend is deepest in the Central Glueckstadt Graben and in the Westholstein trough (Fig. 5j). At the base, the Lower Permian (Rotliegend) contains volcanics and conglomerates, followed upward by 500–1,000 m of upper Rotliegend sedimentary rocks, mainly shale and evaporites (salt). The salt carrying Rotliegend lithology can only be found in the Glueckstadt Graben and adjacent areas.

Below the Rotliegend, the layer of Permo-Carboniferous volcanics (Figs. 5k, 7k) is composed predominantly of rhyolites and andesites (Benek et al. 1996). This unit is very thin over the largest part of the area and thickens toward the north-eastern and south-eastern margins (Fig. 7k). Pre-Permian sediments are strongly compacted clastics that are deepest in the Westholstein trough and in the Central Glueckstadt Graben (Fig. 5l). The thickest pre-Permian sediments are present in the south of the study area (Fig. 7l). Below these pre-Permian sedimentary rocks, the upper crystalline crust has been assumed to be of granitic composition. It has been drilled in areas outside the model and is characterized by seismic p-wave velocities and densities characteristic for this lithology (Yegorova et al. 2008; Maystrenko and Scheck-Wenderoth 2013; Thybo 2001). The top of the crystalline crust is deepest in the middle part of the study area (Fig. 5m) whereas this surface rises to a few 1,000 m at the margins of the Glueckstadt Graben. The thickness map (Fig. 7m) of this layer shows that the thickest upper crystalline crust is

modelled in the northern part of the study area. The lower crystalline crust is interpreted as being of mafic composition in response to observed high seismic p-wave velocities and modelled high densities (Yegorova et al. 2008). Its top is deepest in the north of the study area (Fig. 5n) and the lower crust is thickest in the south-eastern part of the Glueckstadt Graben (Fig. 7n). The crust–mantle boundary (Moho) (Fig. 5o) is shallowest beneath the Central Glueckstadt Graben whereas this interface descends northward and is deepest in the north-east of the study area. The lowermost layer in the model is the lithospheric mantle assumed to consist of peridotite. This layer is thickest beneath the Central Glueckstadt Graben (Fig. 7o) and its base, the lithosphere–asthenosphere boundary deepens towards the north-west (Fig. 5p).

Method

The calculation of the 3D conductive thermal field requires a meshed 3D structural model, which describes the geometry of the main geological units of the study area. Moreover, specific thermal properties for the corresponding units are needed. The applied finite element method implies the assumptions that the basin reached a steady-state condition and that conductive heat transfer is the dominant mechanism for heat transport. The actual calculation of the temperatures is realized by a 3D finite element method [Bayer et al. 1997; Geo modelling system (GMS)]. The basic heat equation

$$c * \rho * (\delta T/\delta t) = \mathrm{div}\,(\lambda * \mathrm{grad}T) + S$$

with c: heat capacity (J/kgK), ρ: density (kg/m^3), T: temperature (K), t is the time (s), λ: thermal conductivity (W/mK) and S: radiogenic heat production (W/m^3), is solved on every node to obtain the 3D conductive thermal field. Assuming steady-state conditions ($\delta T/\delta t = 0$), the thermal field is only dependent on the thermal conductivity (λ) and the radiogenic heat production (S) of the geological layers (Bayer et al. 1997; Scheck-Wenderoth and Maystrenko 2008) and on the choice of boundary conditions. First calculations were carried out using the thermal properties (λ, S) from previous comparable thermal simulations for adjacent areas of the NE German Basin (Noack et al. 2010, 2012; Bayer et al. 1997; Ondrak et al. 1998; Norden et al. 2008, 2012; Scheck 1997). Validation of the model by comparing the calculated results with datasets of measured borehole temperatures is the last step. In this process of model validation, the thermal properties are adjusted and changed within a reasonable range to improve the fit between observed and modelled temperatures. For data visualization PARAVIEW (Kitware) and Geo modelling system (GMS) are used.

Boundary conditions

Because almost one-third of the study area is covered by sea water, an upper thermal boundary condition of 5 °C (average sea water temperature) has been chosen for the seafloor and the surface onshore. This value is also close enough to the average surface temperature of 8 °C in areas not covered by the sea. Accordingly, the 5 °C isotherm follows the topography which reaches from −37 to 134 m in elevation. Determining the lower boundary condition is more complex, because only limited information about structure, composition, temperature and geometry of the deep subsurface is available (Cacace and Scheck-Wenderoth 2010). Basically, there are two options for setting the lower boundary condition: The use of a free lower boundary condition in terms of prescribing a certain heat flow at a certain depth or prescribing a certain temperature at a certain depth. Frequently, a heat flow amounting half the surface heat flow is assumed at the level of the Moho discontinuity based on the assumption that half of the heat arriving at the surface is generated in the crust (Kukkonen et al. 1999). On the other hand, it is impossible to constrain the temperature at the level of the Moho, thus a fixed temperature at this level can be ruled out. Moreover, in spite of intensive exploration for oil and gas in the last decades and many academic seismic experiments, the depth configuration of the Moho (Fig. 5o) is still under debate. This is caused by the complex and regionally very thick salt structures in the Glueckstadt Graben, which inhibit a clear imaging of the Moho. While some studies find a partial uplift of the Moho at the borders of Glueckstadt Graben (Dohr et al. 1989), recent studies suggest an almost flat Moho, with an average depth of around 32 km (Yoon et al. 2008). Furthermore, these new results indicate the presence of a high velocity body right above the Moho (Yoon et al. 2008). In response to these disagreements, we refrain from prescribing either a given heat flow or a given temperature at the Moho.

The only physically reasonable lower boundary condition could be the assumption of an isotherm at the lithosphere–asthenosphere boundary (LAB), as the thermal LAB may represent the depth where partial melting of the peridotite starts in response to pressure–temperature conditions. Results from previous lithospheric conductive thermal models based on consistent indications from seismology and gravity support the hypothesis that the LAB is indeed the domain where partial melting starts (Maystrenko and Scheck-Wenderoth 2009; Scheck-Wenderoth and Maystrenko 2008; Eaton et al. 2009). Therefore, we use a fixed boundary condition of 1,300 °C at the depth of the LAB.

Thermal properties

The thermal properties listed in Table 1 represent end-member models of a sequence of 9 different simulations

during which the sensitivity of the results to the parameters assigned has been evaluated. For the first calculation, the thermal properties were taken from literature (Noack et al. 2012; Norden et al. 2008) based on measurements of rock samples and on temperature modelling of the adjacent NE German Basin. Subsequently, these thermal properties were systematically changed during the validation process. The second set of parameters corresponds to the best-fit model.

A robust result of all calculated models is that the Permian salt is characterized by the highest thermal conductivity. This finding is also consistent with lab measurements on rock salt samples (Čermák and Rybach 1982). Also the layers of the crystalline crust are characterized by relatively high thermal conductivities. For both, the values of thermal conductivity for the salt and the crystalline crust, the respective temperature range has been considered (Landolt Börnstein 1960; Čermák and Rybach 1982). Accordingly for the salt, an average value for a temperature range of 1–150 °C has been chosen whereas the values for the crystalline crust have been chosen for a temperature range of 200–400 °C (upper crystalline crust) and 400–600 °C (lower crystalline crust). For the lithospheric mantle an average value for a temperature range of 600–1,300 °C has been assigned. In contrast, the lowest thermal conductivities have been assigned to the younger sedimentary rocks (Cenozoic, Lower Cretaceous and Jurassic).

Likewise, the values for radiogenic heat production have been chosen lithology-dependent. Accordingly, the highest radiogenic heat production has been assigned to the Permo-Carboniferous volcanics (mostly of rhyolitic to andesitic composition), to Buntsandstein (clay, sand and silt) and pre-Permian sediments (clastics) (Benek et al. 1996; Maystrenko and Scheck-Wenderoth 2013). Contrarily, the Permian salt, most of the sediments as well as the mafic lower crust and peridotitic mantle produce far less radiogenic heat.

Validation by measured in situ temperatures

For model validation, the calculated temperatures are compared to temperatures that have been measured in six wells (Kus et al. 2005; Kühn and Günther 2007; Pester et al. 2010; Rodon and Littke 2005; Schöner 2006; Wohlenberg 1979). Figure 8 illustrates temperature gradients measured down to depths of 3 km (well Allermöhe), 5 km (wells Flensburg Z1, Glueckstadt T1, Mittelplate 2, Moelln Tief 1) and 6 km (well Schleswig Z1). The wells are located in different structural domains with respect to the salt walls (Figs. 2, 3). All measured temperatures indicate a slightly higher thermal gradient than the normal average of 30 °C/km though the thermal gradients are characterized

by different slopes in each well. The temperatures obtained in the first calculation using the set of thermal properties taken from literature (Reference model, Table 1 left column) are generally hotter than the measured in situ temperatures. Accordingly, the thermal properties of the geological layers were successively modified in that the thermal conductivity of all layers has been systematically increased and decreased. For the final and best-fit model, the thermal conductivity of the Lower Cretaceous, the Jurassic, the Buntsandstein and the upper crust was reduced, whereas the thermal conductivity of the Keuper, the Upper Cretaceous and the lower crust was increased compared to the reference model (Noack et al. 2012). The calculated temperatures were poorly sensitive to changes of the thermal conductivity of the Jurassic in response to the rather limited thickness of this layer. Although the difference between modelled and measured temperatures is large for the Flensburg well, the modelled temperatures had the best fit to measured in situ temperatures for the other wells (Fig. 2). It appears that the area of the Flensburg well is characterized by specific conditions that are not accounted for with the steady-state conductive approach (Fig. 8).

Results

The results of the calculated conductive thermal field of the Glueckstadt Graben are shown in Figs. 9 and 10 as the calculated temperature distributions for selected depth levels. As expected, the predicted average temperatures are increasing with depth. Thereby, short-wavelength temperature variations can be only found in the upper/sedimentary part of the model (down to a depth of 20 km) and show a spatial correlation with the thickness distribution of the Permian salt.

The supra-salt thermal field

Figure 9a–g illustrates the temperature distribution for the upper sedimentary part. At 1 km depth (Fig. 9a), highest temperatures (up to 59 °C) are modelled above N–S striking walls and diapirs of the Permian salt with the shape of positive anomalies following the pattern of the salt structures. Positive temperature anomalies are particularly pronounced where the salt walls are overlain by less conductive cover sediments. Lower temperatures at 1 km depth are noticeable in the Central Glueckstadt Graben, at the northern margin of the study area and within the Westholstein and Eastholstein troughs (29–45 °C). In addition, relatively lower temperatures occur within salt structures covered by relatively thin sediments. With increasing depth, from 2 to 7 km (Fig. 9b–f), there is a continuous average increase of temperature around the
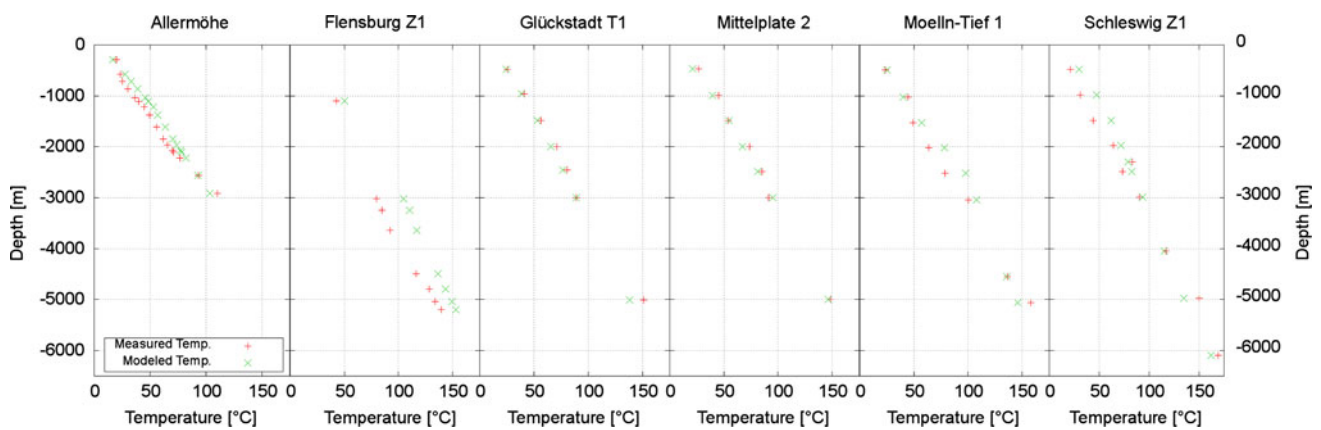
Fig. 8 Comparison of modelled and measured temperatures according to certain depth levels at the 6 wells. Well locations are plotted in Fig. 2

Central Glueckstadt Graben of about 120 °C. In general, relatively lower temperatures occur within salt structures, in the Westholstein trough and in the Central Glueckstadt Graben. The configuration of the highly thermal conductive Permian salt plays an important role for the thermal field in the upper (sedimentary rock) part of the model. In response to the complex structure and the pronounced relief of the salt layer, the predicted conductive thermal field for the sedimentary rocks is complicated by local positive and negative temperature anomalies. Thereby, negative thermal anomalies (of up to 35 °C, Fig. 9g) develop in and underneath thick Permian salt structures.

Figure 11 illustrates the impact of Permian salt structures on the modelled conductive thermal field. In all of the three W–E cross sections (perpendicular to the strike of Permian salt structures) significant variations in calculated temperatures are noticeable, which are caused by the highly conductive Permian salt. Heat is transferred more efficiently throughout the Permian salt, which enhances cooling within these structures. This phenomenon is often described as "chimney effect" (Noack et al. 2010; Kaiser et al. 2011). The effect increases with an increased thickness of salt structures. For this reason negative thermal anomalies (of up to 35 °C) occur underneath thick Permian salt structures where more heat is conducted to the top of the Permian salt layer. If the salt layer is covered by at least 1 km of low conductive sedimentary rocks it comes to a noticeable buildup of heat caused by the insulating effect of the overburden lithologies and the high heat flow entering through the Permian salt. In response to this "chimney effect" positive thermal anomalies (up to 15 °C) evolve above thick Permian salt walls and diapirs, covered by relatively thick sedimentary rocks. Where the cover lithologies are thin, negative thermal anomalies are observed above the salt structures as there the heat is more efficiently transported to the surface than in the insulating clastics at the same depth.

The deep thermal field

At a depth of 10 km (Fig. 9g), the salt-related temperature distribution patterns are still recognizable, though the anomalies are of opposite sign compared to the upper few km: below salt structures negative thermal anomalies are present whereas areas below thick Mesozoic sediments are warmer. Accordingly, relatively warm areas are predicted in the centre and below the eastern flanks of the Central Glueckstadt Graben and below the East Holstein trough (265–270 °C).In addition, colder areas are located at the northern margin of the model and below the Westholstein trough (230–245 °C). The temperature distribution at a depth of 20 km (Fig. 9h) does not correlate anymore spatially with the thickness distribution of the Permian salt (Fig. 7i). As a result, changes in temperature are smooth with a general trend of higher temperatures below the central part of the study area (of up to 426 °C) and colder temperatures at the northern margin of the model (396–404 °C). This pattern correlates spatially with the depth of the top crystalline crust (Fig. 5m). In the northern part of the model, the crystalline crust reaches the shallowest position. As crystalline units have a higher thermal conductivity than sedimentary units, thermal blanketing by sedimentary rocks is less efficient, where modelled units are thinner. On the other hand, within the more conductive crust heat is more efficiently transferred upward. Together these two effects lead to lower temperatures at 20 km depth where the crystalline crust is thick and shallow.

Likewise, in the deeper parts of the model, from 20 to 80 km depth (Figs. 10i–n), the predicted temperature variations are smoothed, maximal temperature variations between 30 and 40 °C are modelled in equal depth. This is due to the fact that in the deeper parts of the model a more or less parallel stratification of layers prevails and thus no abrupt lateral contrasts in thermal conductivity are present. Also the absolute range of temperature variations decreases
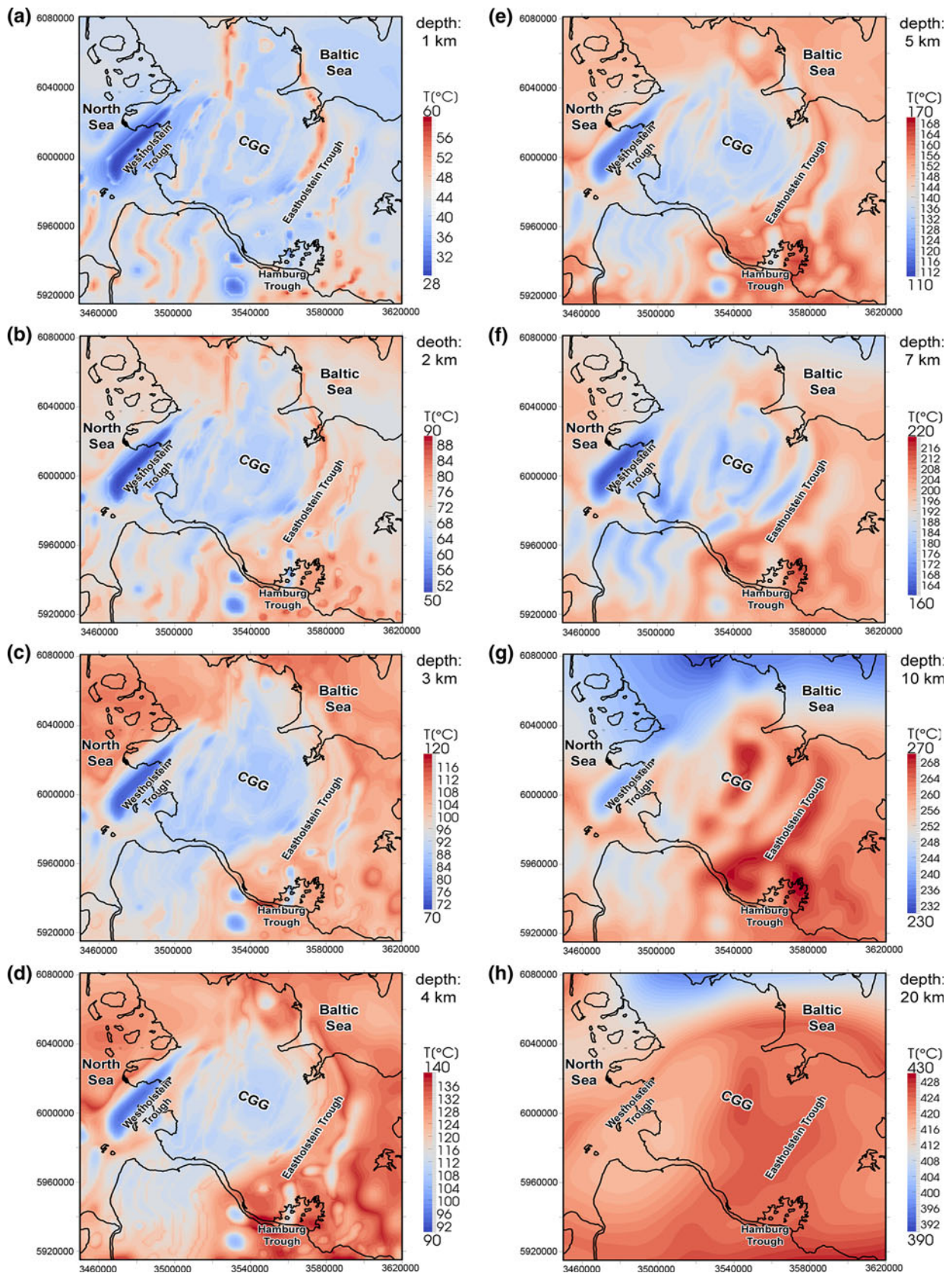
Fig. 9 Temperature distribution for selected depth levels (1–20 km) of the best-fit 3D thermal model. Model coordinates are based on the Gauss-Krueger DHDN (zone 3) system using the WGS 84 datum
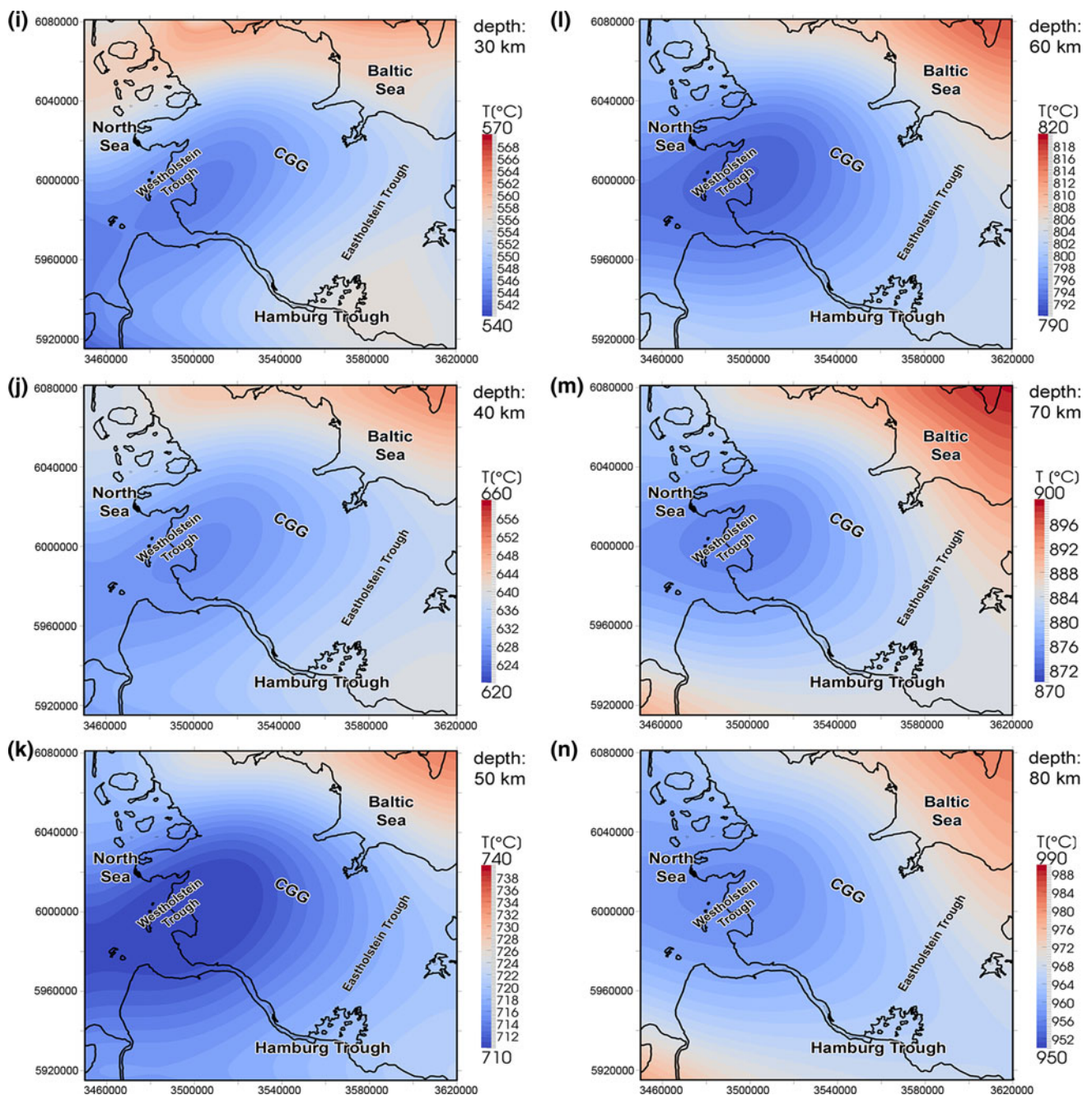
Fig. 10 Temperature distribution for selected depth levels (30–80 km) of the best-fit 3D thermal model. Model coordinates are based on the Gauss-Krueger DHDN (zone 3) system using the WGS 84 datum

with increasing depth though a colder area below the graben is evident compared to warmer domains along the margins of the model. At these larger depths, the calculated temperatures are most sensitive to the configuration of the radiogenic upper crystalline crust (Fig. 5m) and to the depth of the isothermal LAB defining the lower boundary condition in the model. Accordingly, higher temperatures evolve where the radiogenic upper crust is thicker in the upper 30 km. In addition, the shape and topography of the LAB has a major impact on the predicted conductive field

from 40 to 80 km depth. As a result, warm areas are always in the north-east of the study area and match with shallow areas of the LAB.

Discussion

Our results indicate that the spatial temperature distribution in the upper few km of the Glueckstadt Graben is mainly controlled by the topography of salt structures in the
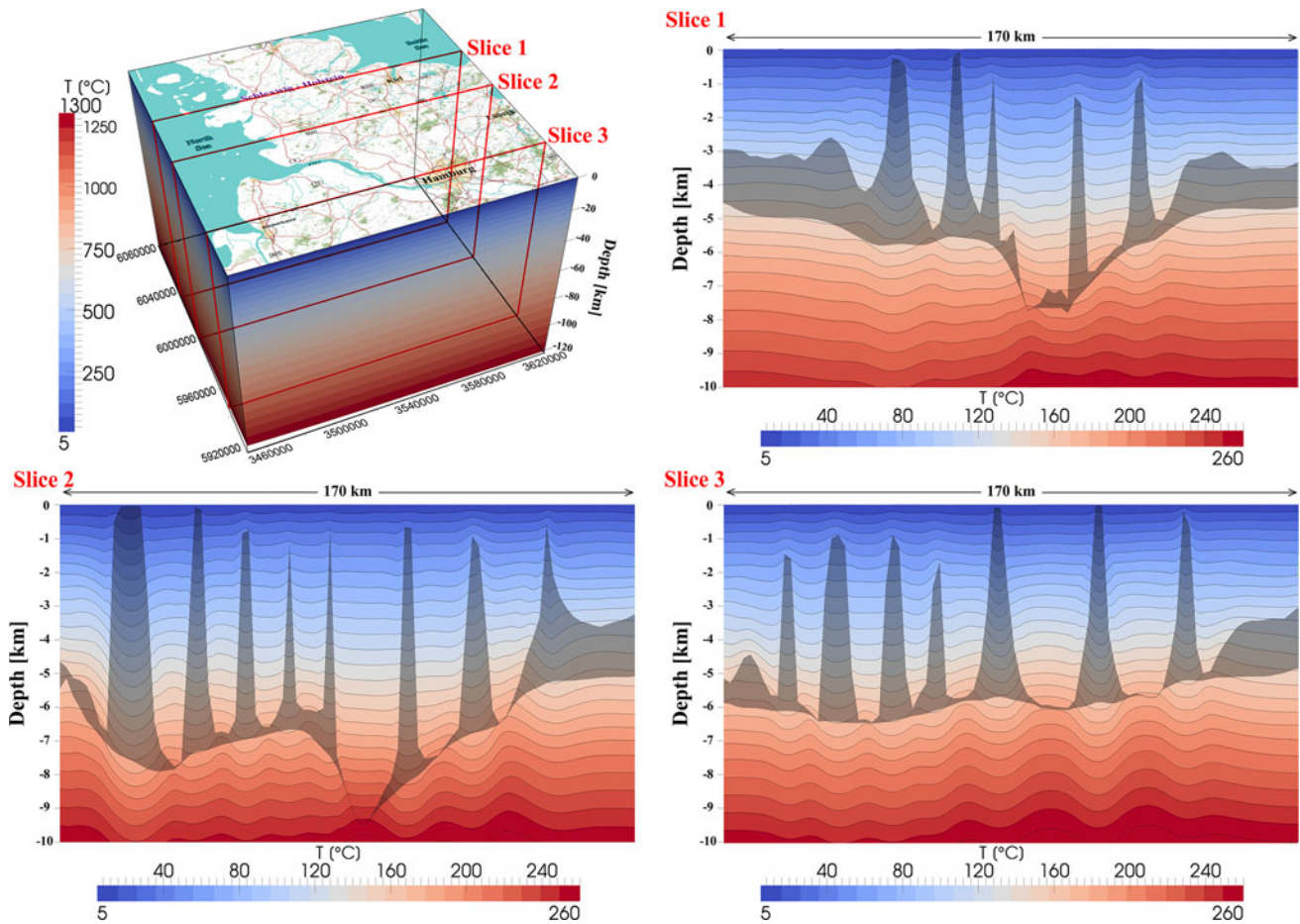
Fig. 11 Cross sections of the upper part of the final thermal model, showing the impact of the grey shaded Permian salt on vertical temperature distribution (vertically exaggerated 1:10)

subsurface and related contrasts in thermal conductivity between conductive salt and insulating cover sediments. Accordingly, the conductive thermal field of the Glueckstadt Graben is strongly controlled by the structure of the highly conductive Permian salt (Zechstein plus salt-rich Rotliegend), causing significant lateral temperature variations for the same reference depth of up to 60 °C (Figs. 9e, f). This unique geological and thermal setting makes the region very interesting for deep geothermal energy utilization. Though we assess only the steady-state conductive thermal field of the Glueckstadt Graben, our results can provide first-order estimates for locations of higher geothermal prospectivity. With the help of this dataset, it is possible to find areas, where high temperatures at shallow depth are expected. This can be imaged for example by the topography of different isotherms throughout the study area. This knowledge can then be used to minimize costs for geothermal drilling projects. Since 100 °C is the minimum temperature for electric power production from geothermal resources, the 100 °C equal temperature map is shown in Fig. 12. The 100 °C isotherm is located at a depth

ranging from 2.3 to 3.8 km. In general, the maximum depth is expected in salt diapirs and salt walls, especially in the west where the isotherm descends down to 3.8 km. In contrast, the minimum depths are located in areas where the Permian salt structures are covered by low conductive younger sediments, which cause increased heat storage. While salt is generally not suitable for extracting hot fluids in response to its impervious nature, the salt margins are filled with permeable sediments. These domains are also characterized by a relatively shallow position of the 100 °C isotherm and could be suitable targets for geothermal exploration.

The validation of the model with the help of a comparison between modelled and measured temperatures showed that the used method (Bayer et al. 1997) is generally valid for the Glueckstadt Graben as a good agreement of modelled and measured temperatures in five of the six used wells is found. Only at the Flensburg well our model always predicts too high temperatures. This can be either related to a local overestimation of the modelled thickness of the high conductive salt or to a local cooling

Fig. 12 Depth distribution map of equal temperature (100 °C). Model coordinates are based on the Gauss-Krueger DHDN (zone 3) system using the WGS 84 datum
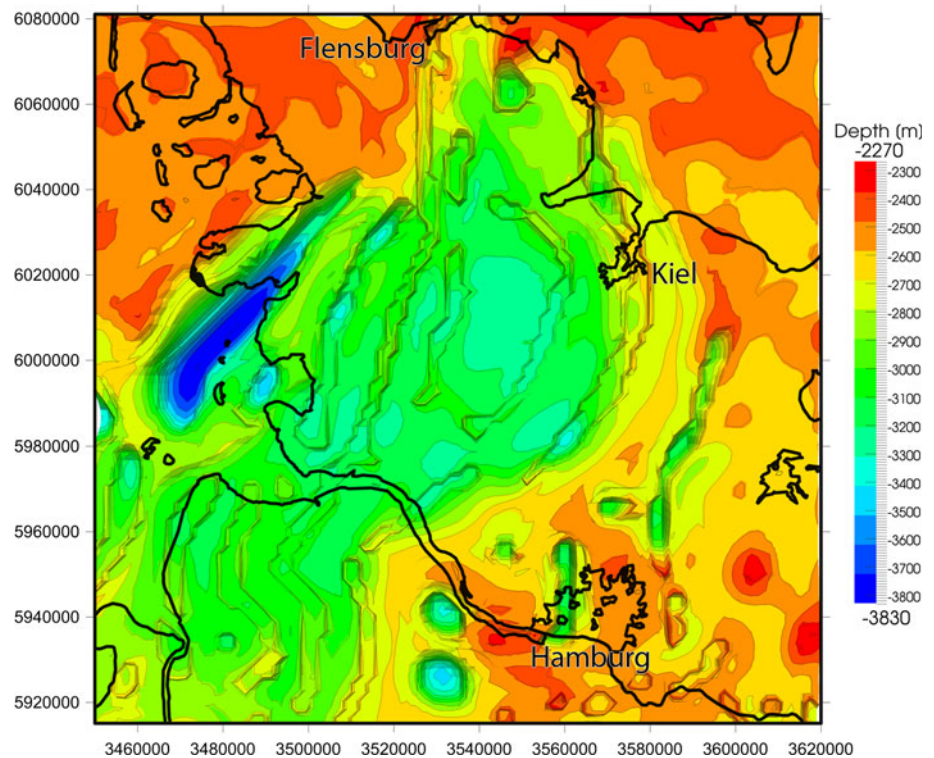
mechanism in this region as for example in response to heat transfer by circulating pore fluids. Moreover, the temperature distribution calculated for the upper part of the 3D model does not consider potential effects of palaeoclimatic changes on subsurface temperatures.

(1) The Flensburg Well was drilled in a small rim syncline, which is next to a salt diapir. The horizontal resolution of the model is 2 km. This can be insufficiently detailed to account for small wavelength irregularities in the structure of the high conductive Permian salt. It might be possible that the model overestimates the thickness of Permian salt at this local point and thus cause a misfit of modelled and measured temperatures.

(2) The model assumes a dominant, laterally uniform lithology within each layer. Small changes in facies are not considered, which might have an influence on the distribution of the thermal properties. Especially, heterogeneities in the Permian salt could have a high impact on the predicted temperatures. It could be that locally less salt is preserved either in the Zechstein or the Rotliegend than considered in the model, thus causing a lower effective conductivity than assumed in the current model.

(3) The Glueckstadt Graben was affected by normal faulting in the past and these normal faults were not considered by the model. Recent studies show that fault permeability might also have an effect on local

temperature distribution (Yousafzai et al. 2010; Cherubini et al. 2013).

(4) Forced groundwater flow induced by lateral variations in hydraulic head can also have a cooling effect on temperatures in the subsurface. In a similar geological setting, in the North-East German Basin, Noack et al. (2013) show that local fluid transport may cause cooling of the shallow thermal field.

(5) Convective heat transport might influence subsurface temperature in this area. The well is located at the west flank of a large impermeable salt diapir. This setting may cause a density driven convective fluid transport in the adjacent permeable sedimentary rocks bringing colder water to greater depth. This could have also an overall cooling effect explaining the measured temperatures.

Conclusions

Our results show that a considerable portion of observed deep temperatures for the Glueckstadt Graben can be explained by a 3D steady-state conductive thermal model. According to the predictions of this model, subsurface temperature in the upper few kilometres of the region is mainly controlled by the configuration of thermally highly conductive Permian salt structures and the related lateral contrasts in thermal conductivity with surrounding and/or

covering less conductive sedimentary rocks. Especially, the upper sedimentary part of the model exhibits large spatial temperature variations, related to the structural features of the relatively highly conductive Permian salt. Thereby, the thickness and geometry of the salt causes two major effects, which enhance the lateral temperature differences. The impact of the "chimney effect" causes an increased heat transport in salt diapirs. As a consequence, positive thermal anomalies develop above salt structures, whereas negative thermal anomalies evolve underneath salt structures.

Apart from these local effects also regional lateral variations in temperature are found. For these regional anomalies the cumulative insulating effects of the entire sediment fill results in a long-wavelength variation of temperatures in response to heat refraction effects caused by the contrast between insulating sedimentary rocks and highly conductive crystalline crust. Finally, the longest wavelength of temperature variations is caused by the depth position of the isothermal lithosphere–asthenosphere boundary defining the regional variations of the overall geothermal gradient.

References

Baldschuhn R, Frisch U, Kockel F (1996) Geotektonischer Atlas von NW-Deutschland 1:300,000. 65 maps, Bundesanstalt für Geowissenschaften und Rohstoffe, Hannover, p. 4

Baldschuhn R, Binot F, Fleig S, Kockel F (2001) Geotektonischer Atlas von Nordwest—Deutschland und dem deutschen Nordsee-Sektor, Reihe A, Heft 153, Geologisches Jahrbuch

Bayer U, Scheck M, Koehler M (1997) Modeling of the 3D thermal field in the northeast German basin. Geol Rundsch 86:241–251. doi:10.1007/s005310050137

Bayer U, Grad M, Pharaoh TC, Thybo H, Guterch A, Banka D, Lamarche J, Lassen A, Lewerenz B, Scheck M, Marotta AM (2002) The southern margin of the East European Craton: new results from seismic sounding and potential fields between the North Sea and Poland. Tectonophysics 360(1–4):301–314. doi:10.1016/S0040-1951(02)00359-1

Benek R, Kramer W, McCann T, Scheck M, Negendank J, Korich D, Huebscher H-D, Bayer U (1996) Permo-Carboniferous magmatism of the Northeast German Basin. Tectonophysics 266(1–4):379–404. doi:10.1016/S0040-1951(96)00199-0

Best G, Kockel F, Schoeneich H (1983) Geological history of the southern Horn graben. Geol Mijnbouw 62:25–33. doi:10.1007/978-94-009-5532-5_2

Brink H, Franke D, Hoffmann N, Horst W, Oncken O (1990) Structure and evolution of the North German Basin. In: Freeman R, Giese P, Mueller S (eds) The European Geotraverse: integrative studies. European Sciences Foundation, Strasbourg, pp 195–212

Brink H, Dürschner H, Trappe H (1992) Some aspects of the late and post-Variscan development of the Northwestern German Basin. Tectonophysics 207(1–2):65–95. doi:10.1016/S0040-1951(02)00359-1

Cacace M, Scheck-Wenderth M (2010) Modeling the thermal field and the impact of salt structures in the North East German Basin. In: Proceedings World Geothermal Congress

Čermák V, Rybach L (1982) Thermal conductivity and specific heat of minerals and rocks. In: Angenheister G (ed) Landolt-Börnstein; Zahlenwerte und Funktionen aus Naturwissenschaften und Technik. (Hrsg.): Bd. 1, Physikalische Eigenschaften der Gesteine, Teilbd. a., Springer-Verlag Berlin, Heidelberg, New York, pp 305–343

Cherubini Y, Cacace M, Scheck-Wenderoth M, Moeck I, Lewerenz B (2013) Controls on the deep thermal field—implications from 3D numerical simulations for the geothermal research site Groß Schönebeck. Environ Earth Sci. doi:10.1007/s12665-013-2519-4

Dohr G, Bachmann G, Grosse S (1989) Das Norddeutsche Becken. Veröffentlichungen-Niedersächsische Akademie der Geowissenschaften 2:4–47

Eaton DW, Darbyshire F, Evans RL, Grütter H, Jones AG, Yuan X (2009) The elusive lithosphere–asthenosphere boundary (LAB) beneath cratons. Lithos 109(1):1–22. doi:10.1016/j.lithos.2008.05.009

Jaritz W (1969) Epiorogenese in Nordwestdeutschland im höheren Jura und in der Unterkreide. Geologische Rundschau 59(1 Taf.):114–124

Jaritz W (1980) Einige Aspekte der Entwicklungsgeschichte der nordwestdeutschen Salzstöcke. Zeitschrift der Deutschen Geologischen Gesellschaft 131:387–408

Kaiser BO, Cacace M, Scheck-Wenderoth M, Lewerenz B (2011) Characterization of main heat transport processes in the Northeast German Basin: Constraints from 3-D numerical models. Geochem Geophys Geosyst 12:Q07011. doi:10.1029/2011GC003535

Kockel F (2002) Rifting processes in NW-Germany and the German North Sea Sector. Geol Mijnbouw 81:149–158

Kühn M, Günther A (2007) Stratabound Rayleigh convection observed in a 4D hydrothermal reactive transport model based on the regional geological evolution of Allermöhe (Germany). Geofluids 7(3):301–312. doi:10.1111/j.1468-8123.2007.00182.x

Kukkonen I, Jokinen J, Seipold U (1999) Temperature and pressure dependencies of thermal transport properties of rocks: implications for uncertainties in thermal lithosphere models and new laboratory measurements of high-grade rocks in the central Fennoscandian shield. Surv Geophys 20(1):59. doi:10.1023/A:1006655023894

Kus J, Cramer B, Kockel F (2005) Effects of a Cretaceous structural inversion and a postulated high heat flow event on petroleum system of the western Lower Saxony Basin and the charge history of the Apeldorn gas field. Neth J Geosci: Geologie en Mijnbouw 84:3–24

Landolt-Börnstein (1960) Zahlenwerte und Funktionen. 6. Auflage, II. Band, Eigenschaften der Materie in ihren Aggregatzuständen. 7. Teil, Elektrische Eigenschaften II (Elektrochemische Systeme) Springer-Verlag, Berlin-Göttingen-Heidelberg 1960. 959 Seiten, Zeitschrift für Elektrochemie, Berichte der Bunsengesellschaft für physikalische Chemie 66(1):74–74

Maystrenko Y, Scheck-Wenderoth M (2009) Density contrasts in the upper mantle and lower crust across the continent–ocean transition: constraints from 3-D gravity modelling at the

Norwegian margin. Geophys J Int 179:1. doi:10.1111/j.1365-246X.2009.04273.x

Maystrenko YP, Scheck-Wenderoth M (2013) 3D lithosphere-scale density model of the Central European Basin system and adjacent areas. Tectonophysics. doi:10.1016/j.tecto.2013.04.023

Maystrenko Y, Bayer U, Scheck-Wenderoth M (2005a) The Glueckstadt Graben, a sedimentary record between the North and Baltic Sea in north Central Europe. Tectonophysics 397(1–2): 113–126. doi:10.1016/j.tecto.2004.10.004

Maystrenko Y, Bayer U, Scheck-Wenderoth M (2005b) Structure and evolution of the Glueckstadt Graben due to salt movements. Int J Earth Sci 6:799–814. doi:10.1007/s00531-005-0003-4

Maystrenko Y, Bayer U, Scheck-Wenderoth M (2006) 3D reconstruction of salt movements within the deepest post-Permian structure of the Central European Basin system—the Glueckstadt Graben. Neth J Geosci: Geologie en Mijnbouw 85(3):181–196

Maystrenko YP, Bayer U, Scheck-Wenderoth M (2013) Salt as a 3D element in structural modelling—example from the Central European Basin system. Tectonophysics 591:62–82. doi:10.1016/j.tecto.2012.06.030

Noack V, Cherubini Y, Scheck-Wenderoth M, Lewerenz B, Höding T, Simon A, Moeck I (2010) Assessment of the present-day thermal field (NE German Basin)—inferences from 3D modelling. Chem Erde 70(Suppl 3):47–62. doi:10.1016/j.chemer.2010.05.008

Noack V, Scheck-Wenderoth M, Cacace M (2012) Sensitivity of 3D thermal models to the choice of boundary conditions and thermal properties: a case study for the area of Brandenburg (NE German Basin). Environ Earth Sci 67(6):1695–1711. doi:10.1007/s12665-012-1614-2

Noack V, Scheck-Wenderoth M, Cacace M, Schneider M (2013) Influence of fluid flow on the regional thermal field: results from 3D numerical modelling for the area of Brandenburg (North German Basin). Environ Earth Sci. doi:10.1007/s12665-013-2438-4 (in press)

Norden B, Förster A, Balling N (2008) Heat flow and lithospheric thermal regime in the Northeast German Basin. Tectonophysics 460:215–229. doi:10.1016/j.tecto.2008.08.022

Norden B, Förster A, Behrends K, Krause K, Stecken L, Meyer R (2012) Geological 3-D model of the larger Altensalzwedel area, Germany, for temperature prognosis and reservoir simulation. Environ Earth Sci 67:511–526. doi:10.1007/s12665-012-1709-9

Ondrak R, Wenderoth F, Scheck M, Bayer U (1998) Integrated geothermal modeling on different scales in the Northeast German basin. Geol Rundsch 87(1):32–42. doi:10.1007/s005310050187

Pester S, Agemar T, Alten J-A, Kuder J, Kuehne K, Maul A–A, Schulz R (2010) GeotIS—the geothermal information system for Germany. In: Proceedings World Geothermal Congress, pp 25–29

Rodon S, Littke R (2005) Thermal maturity in the Central European Basin system (Schleswig-Holstein area): results of 1D basin modelling and new maturity maps. Int J Earth Sci 94(5): 815–833. doi:10.1007/s00531-005-0006-1

Sannemann D (1965) Salt-Stock Families in Northwestern Germany. AAPG Bull 49:357

Sannemann D (1968) Salt-stock families in Northwestern Germany. In: Braunstein J, O'Brien G (eds) Diapirism and diapirs. AAPG publication, Tulsa, pp 261–270

Scheck M (1997) Dreidimensionale Strukturmodellierung des Nordostdeutschen Beckens unter Einbeziehung von Krustenmodellen. Technical Report, Geo Forschungs Zentrum Potsdam

Scheck-Wenderoth M, Maystrenko Y (2008) How warm are passive continental margins? A 3-D lithosphere-scale study from the Norwegian margin. Geology 36:419–422

Schöner R (2006) Comparison of Rotliegend sandstone diagenesis from the northern and southern margin of theNorth German Basin, and implications for the importance of organic maturation and migration. PhD thesis University, Jena

Thybo H (2001) Crustal structure along the EGT profile across the Tornquist Fan interpreted from seismic, gravity and magnetic data. Tectonophysics 334(3):155–190. doi:10.1016/S0040-1951(01)00055-5

Trusheim F (1960) Mechanism of salt migration in northern Germany. Assoc Petrol Geol Bull 44:1519–1540

Wohlenberg J (1979) The subsurface temperature field of the Federal Republic of Germany. Schweizerbart, Hannover

Yegorova T, Maystrenko Y, Bayer U, Scheck-Wenderoth M (2008) The Glueckstadt Graben of the North-German Basin: new insights into the structure from 3D and 2D gravity analyses. Int J Earth Sci 97(5):915–930. doi:10.1007/s00531-007-0228-5

Yoon M-K, Baykulov M, Dümmong S, Brink H-J, Gajewski D (2008) New insights into the crustal structure of the North German Basin from reprocessing of seismic reflection data using the common reflection surface stack. Int J Earth Sci 97(5):887–898. doi:10.1007/s00531-007-0252-5

Yousafzai A, Eckstein Y, Dahl P (2010) Hydrochemical signatures of deep groundwater circulation in a part of the Himalayan foreland basin. Environ Earth Sci 59(5):1079–1098. doi:10.1007/s12665-009-0099-0

Ziegler P (1992) European Cenozoic rift systems. Techtonophysics 208:91–111. doi:10.1016/0040-1951(92)90338-7